Influence of the Poisson effect on the stress dependence of the elastic moduli of soil

Géotechnique Letters **00**, 1–5, http://dx.doi.org/10.1680/geolett.XX.XXXXX

Influence of the Poisson effect on the stress dependence of the elastic moduli of soil

S. CONSTANDINOU* and K. J. HANLEY*

Effective medium theory and discrete-element method (DEM) simulations of smooth spheres both fail to correctly capture the small-strain stiffness of soil. The inability of the latter to capture small-strain stiffness can be overcome by adopting a rough-surface contact model which includes the effect of asperity deformation. Hertzian spheres are commonly used in DEM which neglect the Poisson effect, i.e., the lateral extension of a sphere orthogonal to an applied load. The hypothesis investigated in this paper is that this omission contributes to the inability of smooth-sphere DEM simulations to correctly capture the stress dependence of the elastic moduli of soil. This hypothesis was investigated using the finite-element method. At low to moderate confining stresses, the Poisson effect has little influence on the response. The Poisson effect becomes significant only at confining stresses on the order of 100 MPa, using parameters appropriate for a silica sand: stresses at which massive particle crushing would be expected. At lower stresses, rough-surface contact models remain the most justifiable way to match the stress–stiffness response measured in laboratory testing using DEM simulations.

KEYWORDS: stiffness; elasticity; numerical modelling; finite-element modelling

NOTATION

a	radius of contact area from sphere compression
E	Young's modulus
F	contact force
G_0	elastic (small-strain) shear modulus
K	bulk modulus
K_0	elastic (small-strain) bulk modulus
m	exponent in G_0–σ' relationship
n	exponent in K_0–σ' relationship
R	particle radius
s	deformation (or DEM overlap) of a sphere
$U(R)$	lateral extension at central diameter of sphere
$\delta\epsilon_v$	logarithmic volumetric strain increment
$\delta\sigma'$	increment of effective confining stress
ν	Poisson's ratio
σ'	effective confining stress
$\overline{\sigma}_b$	average stress along each rigid boundary

INTRODUCTION

The elastic or small-strain shear modulus of soil, G_0, depends on the effective confining stress, σ', as do the elastic bulk modulus and Young's modulus. Considering the relation $G_0 \propto \sigma'^m$, experiments have found that $m \approx 1/2$ for many real soils. However, theoretical analyses based on effective medium theory (EMT) have consistently found $m = 1/3$ for a range of regular and random packings, matching analytical solutions for smooth spheres with Hertzian interactions (Duffy & Mindlin, 1957; Walton, 1987; Chang *et al.*, 1991; Santamarina & Cascante, 1996; McDowell & Bolton, 2001). A nonlinear contact interaction, e.g., based on Hertz, is required to capture the stress dependence of the elastic moduli (Yimsiri & Soga, 2000). The limitations of EMT for capturing the variation of the bulk modulus, K, of soft two-dimensional particle assemblies were recently highlighted by Cantor *et al.* (2021). Goddard (1990) proposed two mechanisms to explain the discrepancy between theoretical analyses and experiments which were investigated by McDowell & Bolton (2001): (i) the presence of conical asperities at real interparticle contacts; (ii) an increasing number of contacts with increasing confining stress due to the buckling of force chains.

Discrete-element method (DEM) simulations naturally incorporate the second mechanism. In addition, micro-mechanical expressions have been developed for the elastic moduli which incorporate the coordination number, allowing for a varying number of contacts (Agnolin & Roux, 2007). Allowing the number of interparticle contacts to vary improves agreement with experimental data compared to EMT (Makse *et al.*, 1999). However, buckling is irreversible and not strictly applicable to elastic soil (McDowell & Bolton, 2001).

Manuscript received. . .
Published online at www.geotechniqueletters.com
*School of Engineering, Institute for Infrastructure and Environment, The University of Edinburgh, Edinburgh, EH9 3JL, UK. Corresponding author: K. J. Hanley (k.hanley@ed.ac.uk)

Furthermore, this mechanism is ineffectual for idealised packings of monosized spheres in which new contacts cannot form. Rough-surface DEM contact models have been proposed to account for the first mechanism, e.g., Yimsiri & Soga (2000) and Otsubo *et al.* (2017), the latter building on the work of Cavarretta *et al.* (2010) and O'Donovan *et al.* (2015). These models succeed in increasing m in the $G_0 \propto \sigma'^m$ relationship and enable good agreement with experimental data at low to moderate confining stresses.

One of the key assumptions of Hertzian mechanics (Hertz, 1882) is very small deformations (Dintwa *et al.*, 2008). At high confining stresses, at which $m \approx 1/3$ for rough-surface contact models, the validity of the theory proposed by Hertz becomes questionable. Tatara (1991) extended Hertz's theory for one special case: uniaxial compression of a single unbreakable sphere to large strains between two rigid platens. The extended theory developed by Tatara (1991) includes the lateral extension of the sphere at its equator due to the Poisson effect to give an oblate spheroid. This lateral extension is precluded in conventional DEM simulations, i.e., fundamental spheres remain spherical and cannot deform. Therefore, at large strains, any cross-sectional area of a uniaxially compressed Hertzian sphere in DEM, and hence its stiffness, is underpredicted.

The hypothesis explored in this paper is that the omission of this lateral extension contributes to the discrepancy between $m \approx 1/2$ for real soil and $m \approx 1/3$ in numerical analyses, particularly at high confining stresses. The finite-element method (FEM) is used to investigate this hypothesis. Firstly, the simulation approach is verified by comparing with the analytical solution of Tatara (1991) for uniaxial compression of a single unbreakable sphere. Then the sphere is isotropically compressed between six platens and the relationship between the small-strain bulk modulus, K_0, and the effective confining stress is explored. This takes the form $K_0 \propto \sigma'^n$, distinguishing between G_0 and K_0 relationships using exponents m and n, respectively.

VERIFICATION BY UNIAXIAL COMPRESSION

The commercial package Abaqus FEA (Dassault Systèmes, 2015) was used to quasi-statically compress a sphere between two rigid platens as shown schematically in Fig. 1. The particle and material parameters match Yimsiri & Soga (2000): radius R of 1 mm, density of 2600 kg m^{-3}, Young's modulus E of 69.6 GPa and Poisson's ratio ν of 0.2. The elasticity is modelled using the inbuilt routine in Abaqus for isotropic materials which requires only E and ν. An octant of the entire sphere was simulated using three planes of symmetry and 15 484 quadratic 'C3D20R' elements as shown in Fig. 2. Compression stopped at 5% axial strain: a common heuristic for the maximum permissible overlap between spheres in DEM simulations. The results of this simulation were compared with the predictions of Hertz (1882) and Tatara (1991). The comparison with the latter allows the reliability of these implicit simulations to be verified

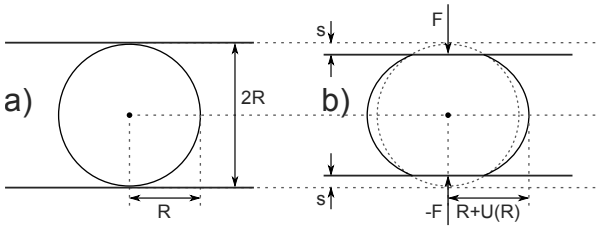

Fig. 1. Schematic showing a single sphere (a) before and (b) after uniaxial compression between rigid platens. Deformations have been exaggerated to enhance clarity of representation

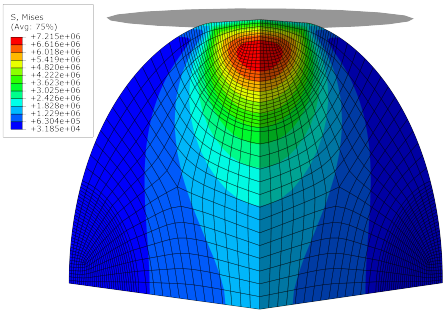

Fig. 2. The octant of the sphere simulated in Abaqus FEA at an axial strain of 5%. The contours represent the von Mises stress measured in kPa.

against an analytical solution developed for non-infinitesimal strains.

According to Hertzian theory, the contact force, F, for a sphere contacting a rigid platen is

$$F = \frac{4E\sqrt{R}}{3\left(1-\nu^2\right)} s^{\frac{3}{2}} \tag{1}$$

where s is the deformation of the sphere (analogous to overlap in a DEM simulation of Hertzian spheres). The equivalent relationship between F and s for the case of linear elasticity is given by equations (2)–(4) in Tatara (1991):

$$s = \frac{F}{E}\left(\frac{3\left(1-\nu^2\right)}{4a} - \frac{c}{\pi}\right) \tag{2}$$

$$a^3 = \frac{3\left(1-\nu^2\right)RF}{4E} \tag{3}$$

$$c = \frac{2(1+\nu)R^2}{\left(a^2+4R^2\right)^{\frac{3}{2}}} + \frac{1-\nu^2}{\sqrt{a^2+4R^2}} \tag{4}$$

where a is the radius of the circular contact area.

The lateral extension at the central diameter of the sphere, $U(R)$, is zero for a Hertzian sphere. For the linear elasticity case, $U(R)$ is given by Tatara (1991) as

$$U(R) = \frac{F(1+\nu)}{\pi E R}\left(\frac{1}{2\sqrt{2}} - (1-2\nu)\left(1-\frac{1}{\sqrt{2}}\right)\right) \tag{5}$$

Both F and $U(R)$ are plotted against axial strain on Fig. 3. The disparity between the FEM force data and the Tatara analytical solution stabilises at around 2% at axial strains beyond 2%. This is considered acceptable for the purposes

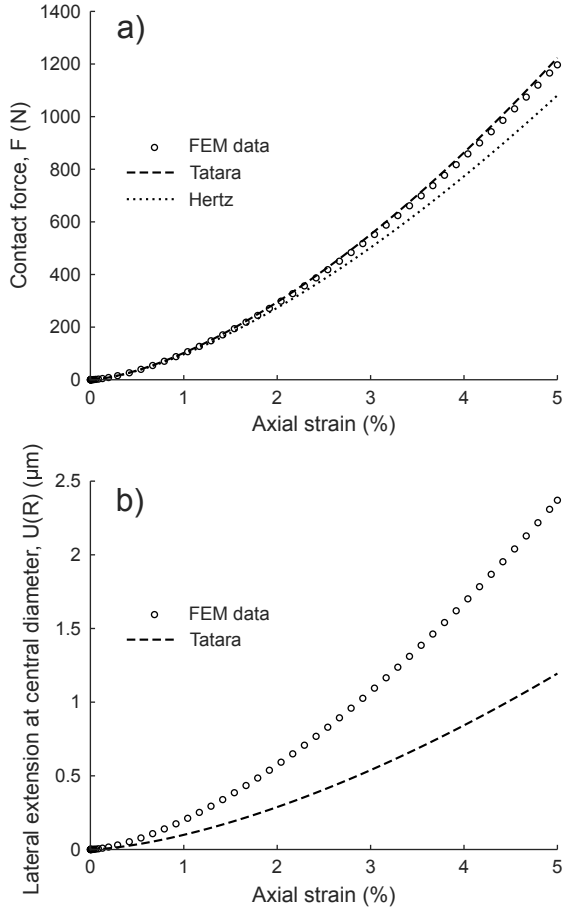

Fig. 3. Relationships between (a) contact force, F, and axial strain and (b) lateral extension at the central diameter of the sphere, $U(R)$, and axial strain for a single sphere subjected to uniaxial compression in FEM, compared with analytical curves of Hertz (1882) and Tatara (1991)

of verification. By contrast, the disparity between the Hertz and Tatara forces increases monotonically with strain, in both absolute and relative terms, as the lateral extension effect becomes significant: the disparity increases in magnitude from 5% at 1% axial strain to 9% at 3% axial strain to 11.7% at 5% axial strain.

While the FEM simulation captures Tatara's analytical F very well, the same is not true of $U(R)$. Fig. 3b shows that $U(R)$ is overestimated by a factor of around two in the simulation compared to equation (5). When Tatara *et al.* (1991) compared their theory with experiments for uniaxial compression of a rubber sphere, they found very good agreement for both F and $U(R)$ up to very large deformations, implying that the disparity in Fig. 3b is attributable to the FEM rather than a deficiency of the analytical prediction. Additional simulations show that the margin of the overestimate in $U(R)$ depends on the Poisson's ratio, e.g., fourfold at $\nu = 0.01$. While the Poisson effect is apparent in FEM, which represents an improvement on Hertzian mechanics for which $U(R) = 0$, it is exaggerated. For the FEM simulations of isotropic compression, the Poisson effect is also likely to be exaggerated.

ISOTROPIC COMPRESSION AND DATA ANALYSIS

Having established the capacity of FEM to predict the contact force for uniaxial compression and display the Poisson effect, albeit more pronounced than the analytical solution of Tatara (1991) indicates, isotropic compression of a sphere between six platens was simulated. The same parameters and octant of a sphere were used as for the uniaxial compression except the Poisson's ratio, ν, was varied from 0.01 to 0.49. Data were exported from the simulations at logarithmically spaced intervals. These data comprised the displacement of each platen from its initial position, s, and the force on each platen. The displacements were identical for each platen; the forces, which were multiplied by four to give the forces for a complete sphere, F, were the same within a small margin of numerical error.

The average stress along each rigid boundary was calculated as

$$\overline{\sigma}_b = \frac{F}{(2R - 2s)^2} \tag{6}$$

The denominator represents the surface area of each rigid boundary enclosing the sphere. Since these average stresses are the same for each boundary, the effective confining stress $\sigma' = \overline{\sigma}_b$. The elastic bulk modulus K_0 was computed as

$$K_0 = \frac{\delta\sigma'}{\delta\epsilon_v} \tag{7}$$

where $\delta\sigma'$ is the increment of effective confining stress and $\delta\epsilon_v$ is the logarithmic volumetric strain increment.

Elastic bulk moduli were also calculated for a single Hertzian sphere compressed between rigid platens following equations (6)–(7). At any effective confining stress σ', $\delta\sigma'$ was fixed at a small value of 100 Pa and $\delta\epsilon_v$ was computed at stresses of $\sigma' \pm 50$ Pa. The corresponding platen displacements, s, were obtained by substituting equation (1) into equation (6) and solving numerically.

RESULTS AND DISCUSSION

Fig. 4 shows the elastic (small-strain) bulk modulus, K_0, against effective confining stress, σ', at Poisson's ratios, ν, of 0.01, 0.1, 0.2, 0.3, 0.4 and 0.49. The range of confining pressures considered, 100 kPa–100 MPa, matches that in Yimsiri & Soga (2000). Linear regressions fit these data very well but are not displayed on Fig. 4 for clarity: the coefficients of determination $R^2 > 0.9975$ for the FEM data, with the lowest R^2 corresponding to the largest Poisson's ratio of 0.49. $R^2 > 0.9999$ for the Hertzian sphere regressions.

As ν increases, so too does K_0 at a fixed σ' for both the FEM and perfect Hertzian spheres. The slopes of the linear regressions, n, increase systematically with increasing ν for the FEM data, from 0.3488 at $\nu = 0.01$ to 0.3650 at $\nu = 0.49$. This is in line with the proposed hypothesis; as the Poisson's ratio increases, the particle expands more due to the increased Poisson effect and so will behave more stiffly when subjected to isotropic compression. The FEM simulations capture, and

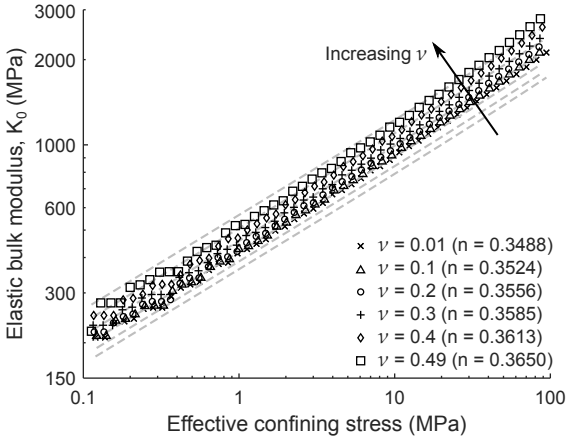

Fig. 4. Elastic bulk modulus, K_0, against effective confining stress, σ', at six Poisson's ratios, ν. The FEM data are shown using black markers; results for a Hertzian sphere are shown as grey dashed lines. The slopes of the best-fit linear regressions to the FEM data, n, are provided in the legend

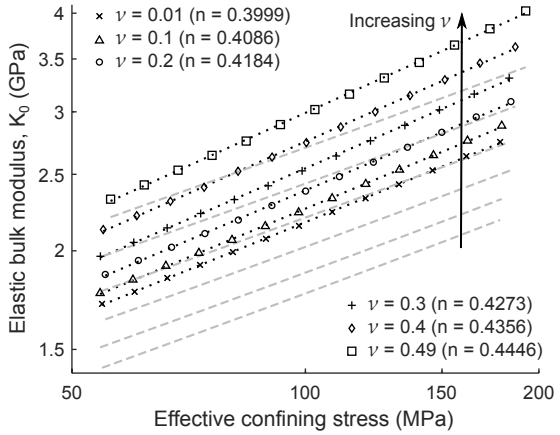

Fig. 5. K_0 against σ' at Poisson's ratios, ν, of 0.01, 0.1, 0.2, 0.3, 0.4 and 0.49 for effective confining stresses of 50 MPa–200 MPa. Black dotted linear regressions are shown for the FEM data (black markers). As for Fig. 4, results for a Hertzian sphere are shown as grey dashed lines

in fact overemphasise, the 'lateral extension' effect (Fig. 3b). For the Hertzian spheres, this effect is absent and n varies negligibly from 0.3388 at $\nu = 0.01$ to 0.3367 at $\nu = 0.49$. Although close, these slopes are not exactly $1/3$ because of significant sphere deformations which violate a key assumption of Hertzian theory. At $\sigma' = 100$ MPa, s ranges from 18.6 µm ($\nu = 0.49$) to 28.6 µm ($\nu = 0.01$): equivalent to 1.86%–2.86% of the sphere's radius. As $s \to 0$, $n \to 1/3$ for the Hertzian spheres.

The Poisson effect is expected to become more pronounced at large strains. This is confirmed in Fig. 5 in which the range of effective confining stresses has been increased to 50 MPa–200 MPa compared to Fig. 4. On Fig. 5, as for Fig. 4, n values for the FEM data increase with increasing ν: from 0.3999 at $\nu = 0.01$ to 0.4446 at $\nu = 0.49$. For all of these regressions, $R^2 > 0.9995$. The equivalent Hertzian spheres significantly underpredict K_0 at these high confining stresses and the regressions have much smaller slopes, ranging from $n = 0.3648$ at $\nu = 0.01$ to $n = 0.3546$ at $\nu = 0.49$.

For real soils, confining stresses of 50 MPa–200 MPa would cause enormous particle crushing even for silica sands (Altuhafi & Coop, 2011; Hanley *et al.*, 2015). Asperities on particle surfaces would certainly be crushed. As a result, rough-surface contact models in DEM analyses of unbreakable spheres become ineffectual at such high stresses. Therefore, the inclusion of the Poisson effect would be a viable option to give a reasonable stress dependency of the elastic moduli. It is questionable, however, whether one should run DEM simulations at such large stresses without including a particle crushing mechanism. At lower stresses, the Poisson effect has a negligible effect; the two mechanisms discussed by Goddard (1990) and McDowell & Bolton (2001) are far more influential. Recalling that the Poisson effect is overestimated in these FEM simulations (Fig. 3b), its effect at low stresses is even less than indicated by Fig. 4. The adoption of rough-surface contact models, e.g., Otsubo *et al.* (2017), remains the most justifiable way of matching experimental measurements using DEM simulations.

While this paper has focused on a single spherical particle, the results are relevant for multi-particle assemblies, even randomly packed ones. The behaviour of a multi-particle assembly is a direct consequence of the behaviours of each individual particle comprising the assembly. Each particle in an idealised cubic packing has an identical stress state so any single particle is representative. Random packings of smooth particles have comparable exponents in the $G_0 \propto \sigma'^m$ relationship (Otsubo *et al.*, 2017). It is also noted that a strictly elastic soil does not allow for sliding at interparticle contacts or buckling of force chains (McDowell & Bolton, 2001). This indicates that contact mechanics is the critical factor for soil elasticity rather than the evolving soil fabric.

CONCLUSIONS

A novel hypothesis was presented and explored in this paper regarding the dependence of the elastic moduli of soil on the effective confining stress, σ'. For real soils, the $G_0 \propto \sigma'^m$ relationship typically has an exponent $m \approx 1/2$; for Hertzian spheres, $m \approx 1/3$. It was hypothesised that the omission of the Poisson effect in Hertzian mechanics contributes to the discrepancy between these exponents, particularly at high confining stresses. By simulating a single spherical particle in FEM, it was found that the Poisson effect has a measurable but very limited influence at low to moderate confining stresses. Using simulation parameters appropriate for a silica sand, the Poisson effect became significant only at confining stresses on the order of 100 MPa. Consequently, rough-surface contact models are far more effective for obtaining a realistic stress dependence of the elastic moduli in DEM simulations.

ACKNOWLEDGEMENTS

The authors would like to thank Dr Francisca Martinez-Hergueta and Dr Stefanos-Aldo Papanicolopulos of the

University of Edinburgh for their advice on the FEM modelling. This work was supported by the UK Engineering and Physical Sciences Research Council (EPSRC) grant EP/R005877/1.

SUPPLEMENTARY INFORMATION

All of the isotropic compression data presented in this paper can be accessed at the following link: https://doi.org/10.7488/ds/3149.

REFERENCES

Agnolin, I. & Roux, J.-N. (2007). Internal states of model isotropic granular packings. III. elastic properties. *Phys. Review E* **76**, 061304.

Altuhafi, F. N. & Coop, M. R. (2011). The effect of mode of loading on particle-scale damage. *Soils Found.* **51**, No. 5, 849–856.

Cantor, D., Cárdenas-Barrantes, M., Preechawuttipong, I., Renouf, M. & Azéma, E. (2021). Bulk modulus of soft particle assemblies under compression. *EPJ Web Conf.: Powders & Grains 2021* **249**, 14014.

Cavarretta, I., Coop, M. & O'Sullivan, C. (2010). The influence of particle characteristics on the behaviour of coarse grained soils. *Géotechnique* **60**, No. 6, 413–423.

Chang, C. S., Misra, A. & Sundaram, S. S. (1991). Properties of granular packings under low amplitude cyclic loading. *Soil Dynamics and Earthquake Engng* **10**, No. 4, 201–211.

Dassault Systèmes (2015). *Abaqus/Standard User's Manual, Version 2016*. Johnston, RI, USA: Simulia Corp.

Dintwa, E., Tijskens, E. & Ramon, H. (2008). On the accuracy of the Hertz model to describe the normal contact of soft elastic spheres. *Granular Matter* **10**, No. 3, 209–221.

Duffy, J. & Mindlin, R. D. (1957). Stress–strain relations and vibrations of a granular medium. *J. Appl. Mech., ASME* **24**, No. 4, 585–593.

Goddard, J. D. (1990). Nonlinear elasticity and pressure-dependent wave speeds in granular media. *Proc. R. Soc. A: Math., Phys. Engng Sci.* **430**, No. 1878, 105–131.

Hanley, K. J., O'Sullivan, C. & Huang, X. (2015). Particle-scale mechanics of sand crushing in compression and shearing using DEM. *Soils Found.* **55**, No. 5, 1100–1112.

Hertz, H. R. (1882). Über die Beruhrüng fester elastischer Körper. *Journal fur die Reine und Angewandte Mathematik* **92**, 156–171, (in German).

Makse, H. A., Gland, N., Johnson, D. L. & Schwartz, L. M. (1999). Why effective medium theory fails in granular materials. *Phys. Review Lett.* **83**, No. 24, 5070–5073.

McDowell, G. & Bolton, M. (2001). Micro mechanics of elastic soil. *Soils Found.* **41**, No. 6, 147–152.

O'Donovan, J., O'Sullivan, C., Marketos, G. & Muir Wood, D. (2015). Analysis of bender element test interpretation using the discrete element method. *Granular Matter* **17**, No. 2, 197–216.

Otsubo, M., O'Sullivan, C., Hanley, K. J. & Sim, W. W. (2017). The influence of particle surface roughness on elastic stiffness and dynamic response. *Géotechnique* **67**, No. 5, 452–459.

Santamarina, J. C. & Cascante, G. (1996). Stress anisotropy and wave propagation: a micromechanical view. *Can. Geotech. J.* **33**, No. 5, 770–782.

Tatara, Y. (1991). On compression of rubber elastic sphere over a large range of displacements – Part 1: Theoretical study. *J. Eng. Mater. – T. ASME* **113**, No. 3, 285–291.

Tatara, Y., Shima, S. & Lucero, J. C. (1991). On compression of rubber elastic sphere over a large range of displacements – Part 2: Comparison of theory and experiment. *J. Eng. Mater. – T. ASME* **113**, No. 3, 292–295.

Walton, K. (1987). The effective elastic moduli of a random packing of spheres. *J. Mech. Phys. Solids* **35**, No. 2, 213–226.

Yimsiri, S. & Soga, K. (2000). Micromechanics-based stress–strain behaviour of soils at small strains. *Géotechnique* **50**, No. 5, 559–571.